HHS Public Access

Author manuscript

Doc Ophthalmol. Author manuscript; available in PMC 2017 July 27.

Published in final edited form as:

Doc Ophthalmol. 2012 June ; 124(3): 163–175. doi:10.1007/s10633-012-9317-2.

Age-related changes in *Cngb1*-X1 knockout mice: prolonged cone survival

Youwen Zhang,
Department of Vision Sciences, University of Alabama at Birmingham, 1670 University Blvd., VH346, Birmingham, AL 35294-0019, USA

Glen R. Rubin,
Department of Vision Sciences, University of Alabama at Birmingham, 1670 University Blvd., VH346, Birmingham, AL 35294-0019, USA

Naomi Fineberg,
Department of Biostatistics, University of Alabama, at Birmingham, Birmingham, AL 35294, USA

Carrie Huisingh,
UAB Center for Clinical and Translational Science, University of Alabama at Birmingham, Birmingham, AL 35294, USA

Gerald McGwin,
UAB Center for Clinical and Translational Science, University of Alabama at Birmingham, Birmingham, AL 35294, USA

Department of Epidemiology, University of Alabama at Birmingham, Birmingham, AL 35294, USA

Steven J. Pittler, and
Department of Vision Sciences, University of Alabama at Birmingham, 1670 University Blvd., VH346, Birmingham, AL 35294-0019, USA

Timothy W. Kraft
Department of Vision Sciences, University of Alabama at Birmingham, 1670 University Blvd., VH346, Birmingham, AL 35294-0019, USA

Abstract

The rod photoreceptor cGMP-gated cation channel has an essential role in phototransduction functioning as the primary point for calcium and sodium entry into the rod outer segment. The channel consists of two subunits, α and β. The α-subunit can function in isolation as an ion channel, and the β-subunit modulates channel activity and has a structural role. We previously reported that a mouse knockout (KO) of the β-subunit and related glutamic acid–rich proteins (GARPs) attenuates rod function and causes structural alterations and slowly progressive retinal degeneration. Here, we have extended our functional analyses of the KO mice evaluating rod and cone function using the electroretinogram in mice up to 4 months of age. Retinal stratification is preserved in the knockout mice at 3 months, and a significant number of cones remain up to 7

Correspondence to: Timothy W. Kraft.
Youwen Zhang and Glen R. Rubin contributed equally.

months based on PNA staining of cone sheaths. Electroretinography of KO mice at 1 month old revealed a diminished dark-adapted b-wave and normal light-adapted b-wave compared to wild-type mice. Over the next 3 months, both dark- and light-adapted b-wave amplitudes declined, but the reduction was greater for dark-adapted b-wave amplitudes. In one-month-old mice, the critical flicker frequency (CFF) was substantially lower for the KO mice at scotopic intensities, but normal at photopic intensities. CFF values remained stable in the KO mice as the b-wave amplitudes decreased with age. Declining b-wave amplitudes confirm an RP phenotype of rod followed by cone degeneration. Flicker responses show that the cone circuits function normally at threshold despite significant losses in the maximum light-adapted b-wave amplitude. These results confirm that rods are marginally functional in the absence of the β-subunit and in addition show that CFF may be a more sensitive measure of remaining functional cone vision in animal models of RP undergoing progressive rod-cone degeneration.

Keywords

Cngb1; Cone; ERG; Flicker; Knockout mice; Light-adapted

Introduction

Rod and cone photoreceptor-specific cyclic nucleotide-gated (CNG) channels reside on the plasma membrane and are critical to phototransduction [1, 2]. The binding of cGMP to CNG channel subunits keeps the channels open in the dark. A circulating ‘dark current’ maintains the photoreceptors in a relatively depolarized state [3]. When light activates the rod and cone pigments, a series of biochemical events ensues that leads to the hydrolysis of cGMP and closure of cGMP-gated channels. Closed channels interrupt the inward Na^+ and Ca^{2+} current causing a hyperpolarization of the photoreceptors, detectable as a corneal negative a-wave in ERG recordings [4, 5]. A positive reflecting b-wave that follows the a-wave mainly reflects on-bipolar cell responses [6–8].

The rod photoreceptor cyclic nucleotide-gated cation channel (CNGC1) is composed of α (CNGA1) and β (CNGB1) subunits with a stoichiometry of 3a:1b [9–11]. While the α-subunit can form functioning homomeric ion channels when expressed alone in heterologous systems, the β-subunit expressed individually does not form a functional channel. Coexpression of the α-subunit with the β-subunit in a heterologous system generates channels closely resembling the native rod channel [12–15]. Native and coexpressed channels relative to homomeric α channels display a flickery open state, are 100 times more sensitive to the Ca^{2+} channel blocker L-*cis*-diltiazem, have increased permeability to divalent ions (Ca^{2+} blockage), exhibit greater ionic selectivity, are modulated by Ca^{2+}-calmodulin (CaM), and show greater fractional activation by cAMP [12, 13, 16]. Thus, the β-subunit confers dramatic adaptability to the native channel.

The β-subunit has an unusual bipartite structure consisting of an N-terminal glutamic acid–rich protein (GARP) region and a C-terminal channel-like region [12]. Two related soluble proteins, GARP1 and GARP2, are also expressed from the *Cngb1* locus encoding the β-subunit. We previously reported a *Cngb1*-X1 knockout mouse model with exon 1 and exon 2

deletion [17]. In this model, the β-subunit and related GARP proteins are not expressed. Another β-subunit knockout mouse that targeted only the channel-like region has also been reported [18]. This model designated here as *Cngb1*-X26 is deleted for exon 26 and does not affect GARP1 or GARP2 expression. Although *Cngb1*-X1 and *Cngb1*-X26 both exhibit degeneration typical of retinitis pigmentosa (RP), differences in phenotype suggest structural and functional roles for GARPs. Rod photoreceptor morphology is better preserved in one-month-old GARP expressing *Cngb1*-X26 knockout mice, yet the single cell and summed ERG responses are not readily detectable in this model. Both models show reduced expression of the α-subunit; however, α-subunit expression is significantly lower in abundance in *Cngb1*-X26 KO mice, which likely accounts for the non-functional rods in these mice. In addition to the difference in α-subunit expression levels, it cannot be ruled out that the functional difference is due to the presence of GARPs exhibiting a dominant negative effect on protein transport in the absence of the β-subunit. GARPs can interact with the CNG channel, peripherin-2/rom-1 oligomers, and phosphodiesterase 6 (PDE6) [19–21].

Gene knockouts that abnormally extend the life of activated rhodopsin or increase opsin concentration result in delayed ERG recovery kinetics [22–25] and have been identified as one possible cause of retinal degeneration [26, 27]. Thus, we have analyzed changes in the ERG and flicker response in order to assess rod and cone function over the first 4 months of life in a *Cngb1*-X1 KO mouse. Our data suggest that rods in the knockout mice are functional, but significantly attenuated and that cone function is initially normal but diminishes in the first 2 months. However, these deficits and their progression do not affect the threshold cone-driven critical flicker frequency (CFF). Thus, CFF is a more sensitive measure of remaining cone function in the KO mice. These mice may be an excellent choice to study the preservation of cones and cone-driven retinal function in an RP model.

Materials and methods

Generation of *Cngb1*-X1 knockout mice

Generation of *Cngb1*-X1 knockout mice was done by in Genious Targeting Laboratory, Inc. (Stony Brook, NY) and has been described in detail [17]. Briefly, a targeting vector p*Cngb1*-KO containing a neomycin resistance (Neo) cassette flanked by *Cngb1* sequence replaced a fragment including exons 1 and 2 and the predicted proximal promoter region. Knockout mice were produced on hybrid backgrounds of C57BL6 and 129SvEv, using a standard homologous recombination methodology. Mice were maintained in compliance with NIH guidelines, as approved by the Institutional Animal Care and Use Committees of the University of Alabama at Birmingham and conform to the ARVO guidelines for the use and care of animals.

Experimental design and basic ERG response recording

All mice used in this study were littermates from heterozygous *Cngb1* +/− parents. Genotypes of litters were determined by PCR as previously described [17]. For each experimental group (beginning at 1 month old), there were at least $n = 11$ animals of each genotype, *Cngb1* −/− (KO), *Cngb1* +/− (HT), or +/+ wild type (WT). ERGs were recorded monthly for each mouse in each group until 4 months of age. Animals were dark-adapted

overnight and anesthetized by intra-peritoneal injection with Avertin 300 μg/g body weight. Both eyes received topical anesthesia (0.5% proparacaine Bausch & Lomb, Tampa, FL). The left eye, which received light stimuli, was dilated with 2.5% phenylephrine (OCuSOFT, Inc., Richmond, TX) and 1% tropicamide (Alcon Laboratories, Inc., Fort Worth, TX). During recordings, the mouse was placed on a 39°C heating pad (Model 39 DP, Braintree Scientific, Inc., Brain-tree, MA) inside a Faraday cage. Head position was stabilized by a bite-bar. Goniosol (Ciba Vision Corp., Duluth, GA) was applied to the corneal platinum wire electrodes. Corneal electrodes were gently placed on the eyes under dim red illumination. The recording electrode was placed on the left eye, and reference electrode was placed on the right eye. A dedicated optical bench focused light from a 100-watt tungsten halogen source onto a fiber optic cable that delivered the light to a 2.2-mm-diameter translucent adaptor into which a platinum wire electrode was embedded [28]. The adaptor was covered by dark nail polish and black rubber on the surrounding surface to eliminate stray light. A brief (2 or 10 ms) stimulus of 505-nm light was attenuated in discreet steps by a set of six Inconel neutral density (ND) filters. A second optical channel delivered saturating light from a camera flash unit that delivered either 5.63×10^4 or 2.2×10^7 R^*/rod. Data were digitized and recorded with National Instrument hardware and software. Total recording time was about 40 min/animal. At each intensity, 3–20 repeated responses were averaged. Interstimulus interval (ISI) ranged between 2.2 and 15.2 s. Light intensities were measured in photons/μm^2 and calculated as log R^* [29].

Isolated light-adapted cone ERG

Rod photoreceptors were saturated by exposure to a 505-nm green conditioning light (bandwidth 35 nm) producing approximately 7300 R^*/rod photoisomerizations per sec. A bright white camera flash producing 5.63×10^4 R^*/rod was delivered on this background in order to elicit the maximal cone ERG, after 30, 120, 210 s of background light exposure.

Sensitivity of ERG rod b-wave

Two methods were used to calculate b-wave sensitivity: (1) The threshold intensity (I) required to evoke a (15 μV) criterion response was calculated. Since our optical bench produced discrete steps of intensity, we assumed linearity and used dim flash responses to calculate sensitivity in μV/(R^* or incident photons). (2) Sensitivity can also be defined as ($I_{1/2}$), which is the light intensity required to evoke a half-maximal b-wave response. $I_{1/2}$ was calculated by fitting an intensity response series with a Naka-Rushton function, $R/R_{max} = I^n/(I^n + k^n)$ [30, 31], where $k = I_{1/2}$. We measured b-wave amplitude from the trough of the a-wave to the peak of the b-wave. Response amplitude was plotted over 8.5 orders of magnitude of light intensity. $I_{1/2}$ was determined in 1-month-old wild type (WT, $n = 5$) and knockout (KO, $n = 5$) mice. The following modifications were made in the ERG recordings to determine sensitivity. The stimulus was decreased from 10 ms to 2 ms. We also increased the flash intensity to 3.39×10^5 R^*/rod for the green camera flash or 2.21×10^7 R^*/rod for the white camera flash to elicit a maximum response (R_{max}) at saturation. Both intensities are greater than the 2.8×10^5 R^*/rod intensity reported as saturating [28]. The interstimulus interval (ISI) was increased with flash intensity, from 2.2 to 30.2 s for regular green flashes, and 1 min 30 s for a green camera flash and 5 min for a white camera flash. Statistical

significance for both dark- and light-adapted b-wave was determined by repeated measures 2-way ANOVA (RM ANOVA) and Tukey's HSD for post-tests.

Recovery of ERG b-wave by multiple flashes

Recovery of the b-wave was determined with respect to the interstimulus interval between flashes. Three 505-nm flashes (bandwidth 35 nm) photoisomerizing 1.7×10^4 *R**/rod were presented in series. The following ISIs were tested: 32, 16, 8, 4, and 2 s. We waited 3 minutes between flash trains, so the total recording time was about 15 min.

Responses to the second and third flashes were averaged, since they were very similar. Recovery was expressed as a percentage ratio by comparing the latter flashes to the response from the first flash for each interval tested. Mice (1-month-old) were divided into three groups: wild type (WT, $n = 16$), heterozygote (HT, $n = 17$), and knockout (KO, $n = 15$) for the recovery experiments. Three to six mice were picked from the 1-month pool to again analyze recovery at 2, 3, and 4 months of age. The recovery ratio in different ISIs of different genotypes was statistically analyzed by repeated measures 2-way ANOVA (RM ANOVA) and Bonferroni for post-tests ($P < .05$) using Graph-Pad, Prism V. 5.

Flicker assessment of rod and cone function

CFF is the flicker frequency at which a stimulus appears steady rather than flickering or pulsing. Electrophysiologically, it is defined as the stimulus frequency for which criterion voltage response amplitudes can be generated. For example, under scotopic conditions, rats can generate a 3-μV response for frequencies up to about 24 Hz [32]. CFF was determined for *Cngb1*-X1 knockout mice in comparison with WT mice in order to assess rod and cone function. ERG recordings were made postnatal (PN) at PN32 ($n = 3$), PN75 ($n = 3$), and PN91 ($n = 3$). The flicker ERG protocol has been described in detail previously [32]. Briefly, a shutter with 6-mm aperture (Uniblitz; Vincent Associates, Rochester, NY) set the stimulation duration to 5 s. A ferro-electric liquid crystal shutter LV050 (Displaytech, Longmont, CO) produced flicker by sinusoidally modulating attenuation. The amplifier (Astro-med CP122 W; Grass Telefactor, W. Warwick, RI) was set to DC. Responses were amplified 2000× and low-pass filtered at 300 Hz. An optical power meter (Graseby Optronics, Orlando, FL) was used to measure the energy output on every experimental day. Average Michelson contrast was 0.86, SD = ± 0.017.

The 5-s light exposure contained between 5 and 200 cycles of the sinusoidally modulated stimulus. The following stimulus frequencies were used: 1, 2, 4, 5, 10, 16, 20, 25, 32, and 40 Hz. The voltage response was approximately sinusoidal mirroring the stimulus. Amplitude of an average one or two cycle response was measured. The $\log_{10}$ of these response amplitudes was plotted versus the stimulus frequency, and the relationship was extrapolated to the 3-μV criterion response and that frequency was defined as CFF for that mean light level [32, 33]. Animals were tested at 12 (WT) or 6 (KO) mean light intensities, ranging from as little as 3.2 photon/μm^2 up to 2×10^6 photon/ μm^2 . KO animals were tested at the six highest mean light levels to measure rod and/or cone function where a response was measurable.

Light microscopy

For light microscopy, following euthanasia eyes were oriented with marker dyes, enucleated, fixed, and embedded in JB-4 as previously described [17]. Four-to 5-μm sections were cut and stained with M-Stain (Polysciences). Slides were visualized with a Nikon E800 microscope using DIC optics and documented with a high-resolution digital camera.

Visualization and counting of peanut agglutinin-labeled cone outer segment sheaths

Rhodamine-tagged peanut agglutinin was used on retinal whole mounts to determine total numbers of cone cells in WT, HT, and KO mice as previously described [34] with modification. Following fixation, and PNA labeling and washing, both eyes of *Cngb1*-X1−/−, +/− and wild-type 129Svev/C57BL/6 J mice were enucleated, oriented at the 12 o'clock point, dorsal of the limbus with a cauterizing iron, and fixed in fresh 4% paraformaldehyde in 0.1 M phosphate buffer (pH 7.4) overnight at 4°C. Following overnight incubation, the cornea, lens, and vitreous were removed, then the optic nerve head was carefully separated from the neuroretina, and the retina was cut in the shape of a Formée Pattée. The retinas were washed 3 × for 15 min in 1 × PB and then incubated in 10% normal goat serum for 1 h, stained overnight at 4°C with rhodamine-conjugated peanut agglutinin (1:400 in 1 × PB, Vector Laboratories), washed again 4× for min. in 1× PB, and mounted on slides w/a fluorescence preservative (fluoromount G, Electron Microscopy Sciences).

Images were then processed in Photoshop by unsharp masking the raw image at 33% then cropping the image to a 200-μm square. Cropped images were batch processed to 8-bit gray scale. Images were counted using the non-plugin version of ImageJ. Images were scaled, brightness/contrasted to maximize counting. Threshold > Auto was selected to highlight structures to be counted. Sliders in Threshold mode were selected to 20/255 to simulate relative photoreceptor shapes. Watershed was used to separate any adjacent photoreceptor structures. Particles were analyzed for an area of 3–12 μM^2 to remove any noise or oblique photoreceptors, and edge counting was excluded. Results were saved as drawings of outlines for the counted images in addition to the measured picture. For low magnification imaging, the whole mounts were visualized through a 2× objective on a Nikon Eclipse E800 M microscope equipped with a 100 W mercury lamp, and images were captured with a SPOT digital camera (Diagnostic Instruments, Inc.) to show the gross view of the entire whole mount. Central and four-quadrant images were taken on an Olympus BX 51 Spinning Disc DSU Confocal using an Olympus 40×/0.95 N.A. UPlanApo objective, Hamamatsu ORCA R^2 camera, and a Tx Red cube (Chroma series 34004) 560/40× excitation//emission 630/60×. Raw images were acquired and deconvolved using the default "no neighbors" setting on SlideBook ver. 5.0. Three 2-month-old mice (6 retinas each) and two 4- or 6- to 7-month-old mice (4 retinas each) per each genotype were analyzed for statistical purposes, comparing the numbers of PNA positive cells in each genotype using a modified Wilcoxon rank sum test and Dunnett multiple comparison test [35]. Data are presented as the median ± SD. $P < 0.05$ was considered statistically significant.

Results

We previously demonstrated that rods in *Cngb1* knockout mice undergo a relatively slow progressive degeneration and all retinal layers are well preserved up to 2 months of age [17]. To demonstrate that retina morphology is maintained at later time points, we examined 3-month-old HT and KO mice. Shown in Fig. 1 is a comparison of a representative region of the retinas of *Cngb1* HT and KO mouse littermates. Mice heterozygous for the KO allele display normal retina stratification in all layers. The KO mice appear grossly normal in thickness in the GCL, IPL, and INL layers. The ONL is reduced to 5–8 rows of nuclei from midperipheral to central retina consistent with known regional variation in layer thickness in normal retinas (representing a 30–40% reduction in cell numbers). Both the ROS and RIS appear shortened. To assess the relative number of cone cells in the knockout mouse, PNA labeling and counting of the PNA-labeled cone sheaths was done. As shown in Fig. 2 (cf. g–k to l–p) and Table 1, cones in 2-month-old mice are present in comparable numbers in all quadrants in WT, HT, and KO mice. The small but significant difference in two WT versus HT regions (Table 1, IT, SN) may reflect the relatively small sample size. Cell counting in five regions of older mice shows that cones are reduced in the KO mice by 6–45% varying by quadrant (Fig. 2g – k to l–p, Table 1). At 6 and 7 months, statistical analysis did not uncover any overall statistically significant differences in cell counts; however, meaningful differences are apparent in inferior knockout retina (42 and 45% reductions in IN and IT regions, respectively) consistent with cone loss observed in a retina degeneration model [34]. While some cone loss is apparent, clearly large numbers of cones are surviving in the knockout retina for up to 7 months.

To assess retina function in the KO mice, we performed electroretinography. Representative 1-month WT and KO dark-adapted ERG traces are shown in Fig. 3a; flash intensities for all recordings were increased from very dim green light on the top to green camera flash on the bottom. Responses in HT mice were comparable to WT (not shown). The maximum b-wave of the KO mouse (485 ± 194) is only 50% that of the WT mouse (964 ± 295) and the KO mouse a-wave (40 ± 19) is less than 12% that of WT mouse(341 ± 141). Based on threshold responses of 35–50 μV, the sensitivity of the KO mouse is about 2.5 log units lower than that of WT mouse. Sensitivity of the entire intensity response function was determined by fitting an average intensity response series from 5 WT and 5 KO mice (Fig. 3b) to a Naka-Rushton function to measure the light intensity required to evoke a half-maximal response ($I_{1/2}$). As judged by $I_{1/2}$, the b-wave was 7.7-times less sensitive ($P < 0.001$) in KO (980 ± 277 photons/μm^2) than WT (127 ± 27 photons/μm^2) mice. We did find an inflection point in the intensity response relation for mid-intensity light (about 2.3 log R^*/rod). Therefore, we fit the lower and upper limbs using the same sigmoid function, selecting 100 R^*/rod as the bordering stimulus intensity point. If the intensity response of the WT mice is fitted with an upper and lower limb Naka-Rushton equations (Fig. 3b red traces) [36, 37], then the $I_{1/2}$ of the upper limb was not different from that of the KO mice. The upper limb is thought to arise from the cone response [37, 38]. The lower limb has a K value of 0.79, and the upper limb has a K value of 3.34, which does not differ in the IR curve from $I_{1/2}$ (K values) of KO mice (2.92 log R^*/rod), suggesting that KO mice have ERG responses dominated by cones, but that a rod component still may be present.

Dark- and light-adapted ERGs were recorded in *Cngb1*-X1 KO ($n = 11$), WT ($n = 12$), and HT ($n = 12$) mice at four time points (1, 2, 3, and 4 months). Figure 4a – c show the relative changes in dark-adapted b-wave amplitudes over time for *Cngb1*-X1 knockout (KO) mice (triangles) compared to wild-type (WT, circles) and heterozygous (HT, squares) mice. The greatly reduced b-wave of KO animals continued to decline as the animals aged, falling to less than 30% of its original amplitude by 4 months of age. Repeated measures Anova analysis indicates no significant differences between WT and HT, but both have b-wave amplitudes that are significantly greater than KO. Also, the KO group decreases over time, while the other two groups increase ($P = 0.001$). The light-adapted b-wave amplitude also declined significantly with age (Fig. 4d, $P = 0.008$). Figure 4e, f show representative ERG waveforms at 1 and 3 months in light-adapted mice. While the b-wave amplitude was normal at 1 month (Fig. 4e), the implicit time for KO animals was significantly longer than WT (46.5 ± 5.7 vs. 38.6 ± 7.2 ms, $P < 0.05$) and remained so over 4 months. The dark- and light-adapted a-wave amplitude in KO mice were eightfold lower than that in WT mice, and the implicit times of the a-waves were delayed in KO mice.

In order to assess the loss of rod vs cone function over the first 4 months of life, we compared the losses of rod + cone (dark-adapted b-wave) versus conealone (light-adapted)-driven signals by using the ratio of light- versus dark-adapted b-wave amplitudes and plotting them as a function of age (Fig. 5). At one month of age, the magnitude of the cone component was relatively large in the KO mice, 205-μV light-adapted b-wave compared to 426 μV for the dark-adapted b-wave. The light/dark ratio for KO mice at 1 month was 48%, compared to WT and HT values of only 26%. This ratio steadily increases over time in the KO mice, while it remained stable in both WT and HT mice, suggesting that rod-driven function declines at a greater rate than cone-driven function. Thus, cone function is declining, but persists over 4 months of life (Table 2).

To measure how quickly the dark-adapted b-wave recovered after a bright flash of light, we examined responses to repeated flashes, decreasing the inter-stimulus interval (ISI) from 32 to 16, 8, 4, and 2 s. There was a 3-min interval between presentations of 3-flash trains in order to prevent light adaptation. Figure 6a shows representative ERG traces for 8- and 32-s ISI for wild-type and KO mice. The response to the first (black line), second (dashed line), and third (gray line) flashes shows little change for a 32-s ISI (right) but incomplete recovery for the 8-s ISI (left). The average recovery of the b-wave is plotted versus the ISI in Fig. 6b. Recovery was near 95% at 32-s ISI for all genotypes; however, at all shorter ISIs, the KO mice showed greater recovery. A similar finding was observed with 4-month-old KO mice (data not shown). Repeated measures ANOVA shows no significant differences between WT and HT and indicates that both groups are recovering significantly less than KO ($P < 0.0001$). The KO group recovers faster than other groups across the range of ISIs ($P < 0.005$). The more complete recovery in the KO group may indicate a faster recovery for the rod-driven response or a greater proportion of cone-driven signals in the dark-adapted b-wave.

Another way to separate the rod and cone components of the ERG is by using the flicker ERG to measure flicker threshold or critical flicker frequency (CFF). The CFF was determined over a broad range of light intensities in wild-type and knockout mice. Figure 7a

shows the CFF versus intensity functions for three WT (filled circles) and three KO (open circles) mice. The results were very consistent from animal to animal within a genotype, but the KO mice were dramatically less sensitive over almost the entire range of intensities used. The KO mice did not generate measurable responses over the lowest three log units of the range tested, consistent with the ERG results. However, at the upper end of our intensity range, the cone-driven CFF of KO mice approached the 40-Hz value seen in WT mice. The CFF function for the KO mice was remarkably stable. Figure 7b shows that the CFF results for PN32 (open circles), PN75 (filled squares), and PN91 (open triangles) are virtually indistinguishable. In fact, for the upper most log unit of our stimuli, the knockout CFF falls within the range of the wild-type values shown in Fig. 7b, where the gray area represents the mean ± one standard deviation. Thus, ERG CFF was dramatically lower or absent at scotopic intensities, yet near normal at photopic intensities, and remarkably it did not decline during the 3 months of testing despite the fact that the light-adapted b-wave maximum response declined 50% in the same period.

Discussion

Rod photoreceptors in *Cngb1*-X1 mice are functional albeit minimally, despite the absence of the β-subunit and a significant reduction in the amount of the α-subunit [17]. This result is consistent with studies in heterologous systems demonstrating α-subunit channel activity in the absence of the β-subunit [14, 15]. The threshold ERG response was raised by 2.5 log units in *Cngb1* KO mouse compared to WT, which however is still 2 log units more sensitive than threshold in the rodless rhodopsin knockout mouse [36]. In the *Cngb1* KO mouse, the dark-adapted a-wave was about 2.5 times larger in amplitude than the light-adapted a-wave, which reflects some rod contribution to the ERG under dark-adapted conditions. These results support previous single cell recordings in 1-month-old KO mice [17], which indicate reduced sensitivity of rods. Additionally, reported findings of two point mutations in the CNGB1 locus in different RP patients indicate early preservation of cone function with some rod function that is lost over time [39, 40]. To date, there have been no reported null mutations in RP patients.

We speculated that the rod-degenerated *Cngb1*-X1 model might have faster kinetics in the dark due to a greater proportion of cone signals. However, the dark-adapted a-wave's implicit time in KO mice was longer than in WT mice, while the timing of the light-adapted a-wave was not significantly different (data not shown). The light-adapted kinetics suggests normal timing in the responses of the cones and cone-driven b-wave in *Cngb1*-X1 mice, which is also confirmed by the normal CFF under photopic conditions. Since the amplitude of the light-adapted a-wave is significantly smaller, the retina degeneration is affecting not only rods, but also cone photoreceptors. PNA staining indicates loss of cones from 6 to 45% in all quadrants and in central retina in 6- and 7-month-old KO mice (Table 1). One could speculate that a smaller cone input in our KO mouse results in the longer implicit times seen under dark-adapted conditions.

Dark-adapted b-wave sensitivity ($I_{1/2}$) demonstrates that KO mice are 8.3-fold less sensitive than WT mice (Fig. 3b), roughly consistent with the 34-fold loss of sensitivity seen in single rod photoreceptor recordings [17]. The remaining fourfold difference could be explained by

the two methods. Single cell recordings measure one ex vivo rod response at a time, whereas the full-field dark-adapted ERG is a massed tissue response recorded in vivo. In addition, the ERG includes the b-wave, contributed primarily by on-rod bipolar cells in the inner retina and therefore includes gain mechanisms in the photoreceptor to bipolar cell synapse.

The maximum dark-adapted b-wave represents a mixed rod and cone response, while the light-adapted b-wave reflects isolated cone activity. Thus, the ratio of the light- to dark-adapted b-wave amplitudes (Fig. 5) indicates the relative strengths of the rod- and conedriven inputs. Following the ratio of these inputs over 4 months indicates whether one circuit is more significantly affected. In the animal model tested here, both circuits are declining with age (Fig. 4a,d). However, the rod-driven function is deteriorating at a faster rate, as demonstrated by the increase in the light-/dark-adapted b-wave ratio over the 4-month period. In contrast, the ratio in the WT and HT mice is stable over time, indicated by the zero slope of the lines in Fig. 5.

The increased recovery to repeated flashes in the KO mouse (Fig. 6) may reflect the proportionally larger cone signal, since cones recover faster. We cannot rule out however that loss of protein interaction due to the absence of GARPs or the β-subunit is also involved. It has recently been shown that both the channel β-subunit N-terminal GARP region and GARP1 and GARP2 can act as gating inhibitors of the CNG channel [41].

It is remarkable that the KO mouse CFF curve is stable over the first 3 months of life (Fig. 7), while over the same time period the dark-adapted maximum b-wave amplitude decreases by over 50% (Fig. 4). The light-adapted b-wave, which represents cone-driven retinal function, declines by nearly half (42%), indicating degeneration of cones, yet the CFF is not only stable, it remains within the range of wild-type CFF values even for the brightest stimulus tested. One explanation for this apparent contradiction is that the two tests are measuring different functional aspects of the cone pathways in the retina. The bright flash on a rod-saturating background tests the maximum conedriven transretinal voltage achievable, while the CFF measures threshold asking “What is the maximum frequency the cone-driven circuitry can follow while generating a minimally detectable transretinal voltage?” The criterion voltage selected was 3 μV. If the behaviorally relevant voltage for flicker detection is more like 30 or 50 μV, then a more pronounced behavioral deficit might be found. The important point to emphasize is that ERG tests of maximum amplitude or maximum current may tell something very different about the retinal integrity than threshold measures testing the same retinal circuits.

We have demonstrated impaired rod function in our Cngb1-X1 KO mice. The dark- and light-adapted ERG responses decline over time in a manner typical of RP (Fig. 4). Although the scotopic flicker response was reduced, we did not find any significant changes to the photopic ERG CFF over the course of our study (Fig. 7). This finding was especially remarkable because the light-adapted b-wave declined 42% in amplitude while CFF was stable. Maximum response amplitudes better reflect degenerative changes; however, the relative maintenance of CFF suggests that preservation of threshold responses may be functionally more important than the maximum response. Thus, CFF may be a better measure of cone circuit function in retinal diseases.

Acknowledgments

We thank Dr. Jeffrey Messinger for assistance with visualization and counting of PNA-labeled cone sheaths, Dr. Leigh Millican for assistance with light and electron microscopy, Dr. Chris Strang for help with whole-mount fluorescence microscopy, and Dr. Yuquan Wen and Alex McKeown for assistance with IGOR software analysis. This work was supported by NIH grant EY018143 to SJP. NIH/NEI supported Vision Sciences Core Modules from grant P30 EY03039 were used to facilitate some of the research results.

References

1. Kaupp UB, Seifert R. Cyclic nucleotide-gated ion channels. Physiol Rev. 2002; 82:769–824. [PubMed: 12087135]
2. Molday RS. Photoreceptor membrane proteins, phototransduction, and retinal degenerative diseases: the Friedenwald lecture. Invest Ophthalmol Vis Sci. 1998; 39:2493–2513.
3. Barnes S. After transduction: response shaping and control of transmission by ion channels of the photoreceptor inner segments. Neuroscience. 1994; 58:447–459. [PubMed: 7513385]
4. Hagins WA, Penn RD, Yoshikami S. Dark current and photocurrent in retinal rods. Biophys J. 1970; 10:380–412. [PubMed: 5439318]
5. Penn RD, Hagins WA. Signal transmission along retinal rods and the origin of the electroretinographic a-wave. Nature. 1969; 223:201–204. [PubMed: 4307228]
6. Gurevich L, Slaughter MM. Comparison of the waveforms of the ON bipolar neuron and the b-wave of the electroretinogram. Vis Res. 1993; 33:2431–2435. [PubMed: 8249322]
7. Hood DC, Birch DG. Beta wave of the scotopic (rod) electroretinogram as a measure of the activity of human on-bipolar cells. J Opt Soc Am A Opt Image Sci Vis. 1996; 13:623–633. [PubMed: 8627419]
8. Robson JG, Frishman LJ. Response linearity and kinetics of the cat retina: the bipolar cell component of the dark-adapted electroretinogram. Vis Neurosci. 1995; 12:837–850. [PubMed: 8924408]
9. Weitz D, Ficek N, Kremmer E, Bauer PJ, Kaupp UB. Subunit stoichiometry of the CNG channel of rod photoreceptors. Neuron. 2002; 36:881–889. [PubMed: 12467591]
10. Zhong H, Molday LL, Molday RS, Yau KW. The heteromeric cyclic nucleotide-gated channel adopts a 3A:1B stoichiometry. Nature. 2002; 420:193–198. [PubMed: 12432397]
11. Zheng J, Trudeau MC, Zagotta WN. Rod cyclic nucleotide-gated channels have a stoichiometry of three CNGA1 subunits and one CNGB1 subunit. Neuron. 2002; 36:891–896. [PubMed: 12467592]
12. Korschen HG, Illing M, Seifert R, Sesti F, Williams A, Gotzes S, Colville C, Muller F, Dose A, Godde M, Molday L, Kaupp UB, Molday RS. A 240 kDa protein represents the complete beta-subunit of the cyclic nucleotide-gated channel from rod photoreceptor. Neuron. 1995; 15:627–636. [PubMed: 7546742]
13. Chen TY, Peng YW, Dhallan RS, Ahamed B, Reed RR, Yau KW. A new subunit of the cyclic nucleotide-gated cation channel in retinal rods. Nature. 1993; 362:764–767. [PubMed: 7682292]
14. Kaupp UB, Niidome T, Tanabe T, Terada S, Bonigk W, Stuhmer W, Cook NJ, Kangawa K, Matsuo H, Hirose T. Primary structure and functional expression from complementary DNA of the rod photoreceptor cyclic GMP-gated channel. Nature. 1989; 342:762–766. [PubMed: 2481236]
15. Dhallan RS, Macke JP, Eddy RL, Shows TB, Reed RR, Yau KW, Nathans J. Human rod photoreceptor cGMP-gated channel: amino acid sequence, gene structure, and functional expression. J Neurosci. 1992; 12:3248–3256. [PubMed: 1379636]
16. Chen TY, Illing M, Molday LL, Hsu YT, Yau KW, Molday RS. Subunit 2 (or beta) of retinal rod cGMP-gated cation channel is a component of the 240-kDa channel-associated protein and mediates Ca(2+)-calmodulin modulation. Proc Natl Acad Sci USA. 1994; 91:11757–11761. [PubMed: 7526403]
17. Zhang Y, Molday LL, Molday RS, Sarfare SS, Woodruff ML, Fain GL, Kraft TW, Pittler SJ. Knockout of GARPs and the beta-subunit of the rod cGMP-gated channel disrupts disk morphogenesis and rod outer segment structural integrity. J Cell Sci. 2009; 122:1192–1200. [PubMed: 19339551]

18. Huttl S, Michalakis S, Seeliger M, Luo DG, Acar N, Geiger H, Hudl K, Mader R, Haverkamp S, Moser M, Pfeifer A, Gerstner A, Yau KW, Biel M. Impaired channel targeting and retinal degeneration in mice lacking the cyclic nucleotide-gated channel subunit CNGB1. J Neurosci. 2005; 25:130–138. [PubMed: 15634774]
19. Korschen HG, Beyermann M, Muller F, Heck M, Vantler M, Koch KW, Kellner R, Wolfrum U, Bode C, Hofmann KP, Kaupp UB. Interaction of glutamic-acid-rich proteins with the cGMP signalling pathway in rod photo-receptors. Nature. 1999; 400:761–766. [PubMed: 10466724]
20. Poetsch A, Molday LL, Molday RS. The cGMP-gated channel and related glutamic acid-rich proteins interact with peripherin-2 at the rim region of rod photoreceptor disc membranes. J Biol Chem. 2001; 276:48009–48016. [PubMed: 11641407]
21. Pentia DC, Hosier S, Cote RH. The glutamic acid-rich protein-2 (GARP2) is a high affinity rod photoreceptor phosphodiesterase (PDE6)-binding protein that modulates its catalytic properties. J Biol Chem. 2006; 281:5500–5505. [PubMed: 16407240]
22. Lyubarsky AL, Chen C, Simon MI, Pugh EN Jr. Mice lacking G-protein receptor kinase 1 have profoundly slowed recovery of cone-driven retinal responses. J Neurosci. 2000; 20:2209–2217. [PubMed: 10704496]
23. Chen CK, Burns ME, Spencer M, Niemi GA, Chen J, Hurley JB, Baylor DA, Simon MI. Abnormal photoresponses and light-induced apoptosis in rods lacking rhodopsin kinase. Proc Natl Acad Sci USA. 1999; 96:3718–3722. [PubMed: 10097103]
24. Nusinowitz S, Nguyen L, Radu R, Kashani Z, Farber D, Danciger M. Electroretinographic evidence for altered phototransduction gain and slowed recovery from photobleaches in albino mice with a MET450 variant in RPE65. Exp Eye Res. 2003; 77:627–638. [PubMed: 14550405]
25. Birch DG, Peters AY, Locke KL, Spencer R, Megarity CF, Travis GH. Visual function in patients with cone-rod dystrophy (CRD) associated with mutations in the ABCA4(ABCR) gene. Exp Eye Res. 2001; 73:877–886. [PubMed: 11846518]
26. Fain GL, Lisman JE. Light, Ca^{2+}, and photoreceptor death: new evidence for the equivalent-light hypothesis from arrestin knockout mice. Invest Ophthalmol Vis Sci. 1999; 40:2770–2772. [PubMed: 10549634]
27. Frasson M, Sahel JA, Fabre M, Simonutti M, Dreyfus H, Picaud S. Retinitis pigmentosa: rod photoreceptor rescue by a calcium-channel blocker in the rd mouse. Nat Med. 1999; 5:1183–1187. [PubMed: 10502823]
28. Lyubarsky AL, Pugh EN Jr. Recovery phase of the murine rod photoresponse reconstructed from electroretinographic recordings. J Neurosci. 1996; 16:563–571. [PubMed: 8551340]
29. Lyubarsky AL, Daniele LL, Pugh EN Jr. From candelas to photoisomerizations in the mouse eye by rhodopsin bleaching in situ and the light-rearing dependence of the major components of the mouse ERG. Vis Res. 2004; 44:3235–3251. [PubMed: 15535992]
30. Birch DG, Fish GE. Rod ERGs in retinitis pigmentosa and cone-rod degeneration. Invest Ophthalmol Vis Sci. 1987; 28:140–150. [PubMed: 3804644]
31. Hood DC, Birch DG. A quantitative measure of the electrical activity of human rod photoreceptors using electroretinography. Vis Neurosci. 1990; 5:379–387. [PubMed: 2265151]
32. Rubin GR, Kraft TW. Flicker assessment of rod and cone function in a model of retinal degeneration. Doc Ophthalmol. 2007; 115:165–172. [PubMed: 17674067]
33. Pinilla I, Lund RD, Sauve Y. Cone function studied with flicker electroretinogram during progressive retinal degeneration in RCS rats. Exp Eye Res. 2005; 80:51–59. [PubMed: 15652526]
34. Li X, Li W, Dai X, Kong F, Zheng Q, Zhou X, Lu¨ F, Chang B, Rohrer B, Hauswirth WW, Qu J, Pang JJ. Gene therapy rescues cone structure and function in the 3-month-old rd12 mouse: a model for midcourse RPE65 leber congenital amaurosis. Invest Ophthalmol Vis Sci. 2011; 52:7–15. [PubMed: 21169527]
35. Rosner B, Glynn RJ, Lee M-LT. Extension of the rank sum test for clustered data: two-group comparisons with group membership defined at the subunit level. Biometrics. 2006; 62:1251–1259. [PubMed: 17156300]
36. Toda K, Bush RA, Humphries P, Sieving PA. The electroretinogram of the rhodopsin knockout mouse. Vis Neurosci. 1999; 16:391–398. [PubMed: 10367972]

37. Peachey NS, Alexander KR, Fishman GA. The luminance-response function of the dark-adapted human electroretinogram. Vis Res. 1989; 29:263–270. [PubMed: 2788958]

38. Herrmann R, Lee B, Arshavsky VY. RGS9 knockout causes a short delay in light responses of ON-bipolar cells. PLoS One. 2011; 6:e27573. [PubMed: 22096596]

39. Bareil C, Hamel CP, Delague V, Arnaud B, Demaille J, Claustres M. Segregation of a mutation in CNGB1 encoding the beta-subunit of the rod cGMP-gated channel in a family with autosomal recessive retinitis pigmentosa. Human Genet. 2001; 108:328–334. [PubMed: 11379879]

40. Kondo H, Qin M, Mizota A, Kondo M, Hayashi H, Hayashi K, et al. A homozygosity-based search for mutations in patients with autosomal recessive retinitis pigmentosa, using microsatellite markers. Invest Ophthalmol Vis Sci. 2004; 45:4433–4439. [PubMed: 15557452]

41. Michalakis S, Zong X, Becirovic E, Hammelmann V, Wein T, Wanner KT, Biel M. The glutamic acid-rich protein is a gating inhibitor of cyclic nucleotide-gated channels. J Neurosci. 2011; 31:133–141. [PubMed: 21209198]

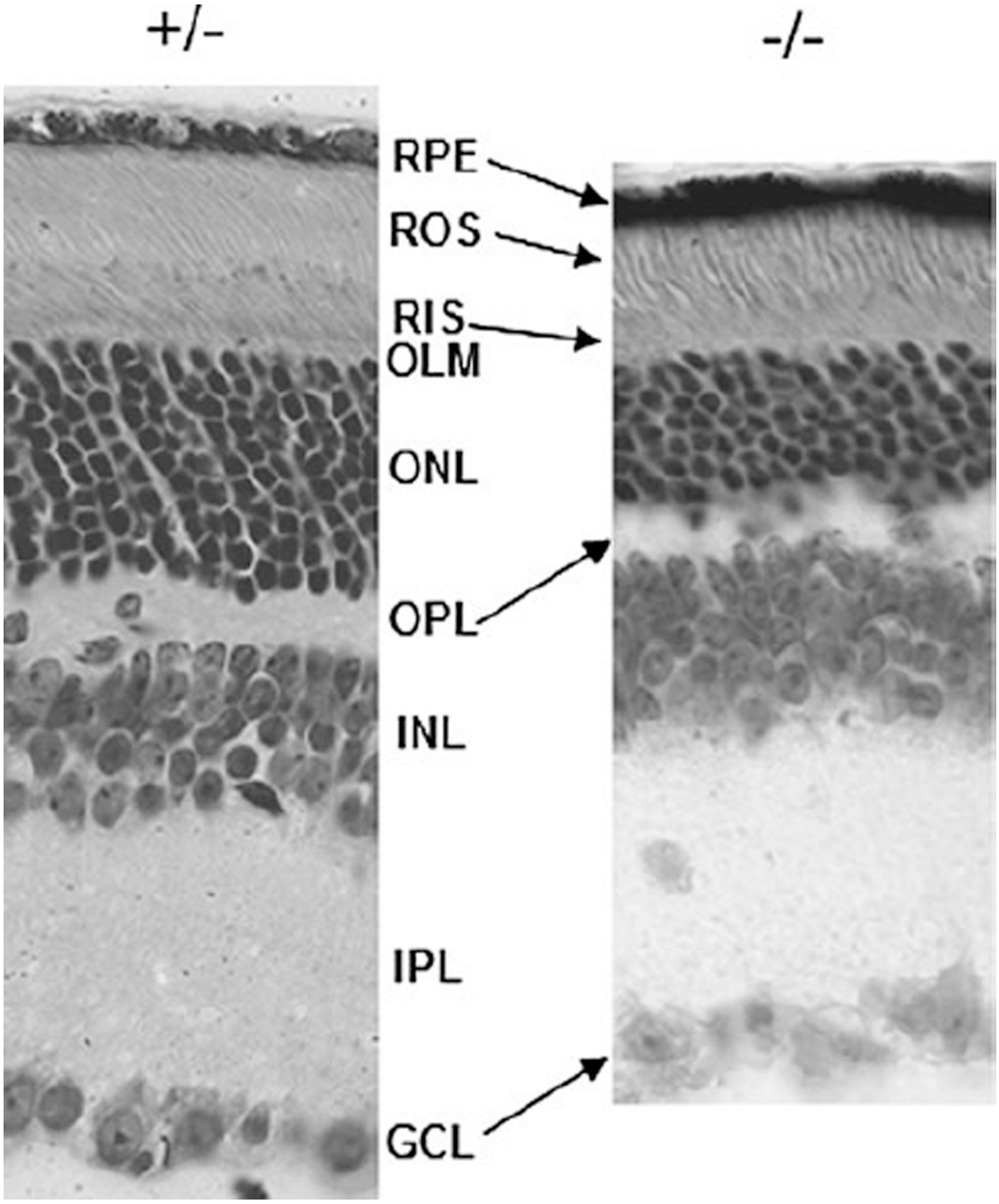

Fig. 1.

Histologic comparison of the retina of 3-month-old heterozygous and homozygous KO mice littermates. Mice heterozygous for the KO allele display normal retina stratification in all layers. The KO mice appear grossly normal in the GCL and inner retina layers. The ONL is reduced to 5–8 rows of nuclei from mid-peripheral to central retina. Both the ROS and RIS appear shortened and disorganized. Sections were cut from mid-central retina in the nasal quadrant and are shown aligned at the OLM (orig. mag. ×400)

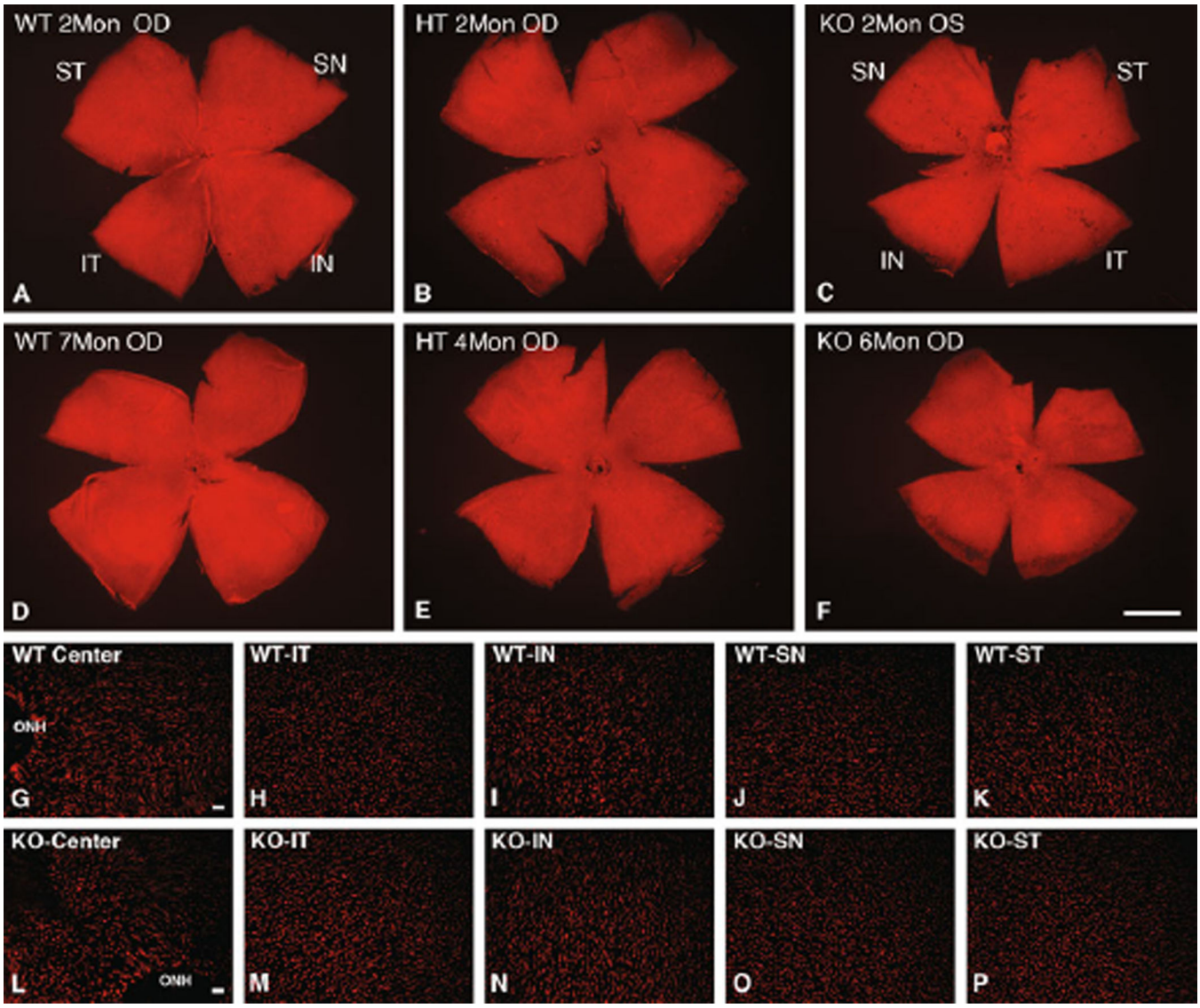

Fig. 2.

Morphometric analysis of PNA-stained cone sheaths. **a–f** Representative whole mounts stained with PNA from 2 to 7 months. Uniform distribution of cone sheaths was observed in WT, HT, and KO mice retina. *Scale bar* in F, 1 mm. (**g–p**) Increased magnification of representative regions of the 2-month retina of (**g–k**) WT and (**l–p**) KO in each of five regions: Center, central including optic nerve head (ONH); *IT* inferior temporal; *IN* inferior nasal; *SN* superior nasal; *ST* superior temporal. *Scale bars* in G, L, 20 μm

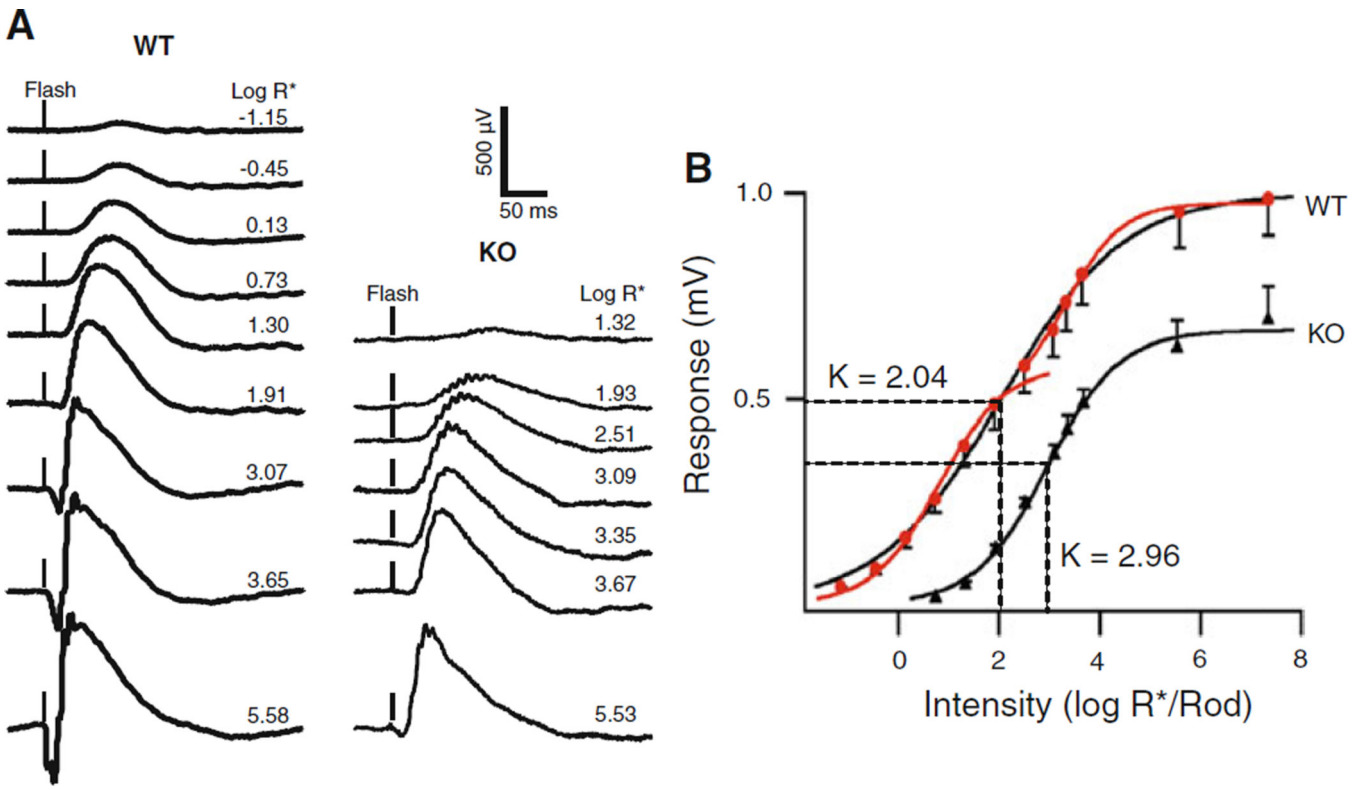

Fig. 3.

ERG intensity response series at PN 30 for *Cngb1*-X1 knockout and wild-type mice. **a** Dark-adapted flash ERGs recorded to 505-nm 2-ms flashes. Flash intensity increases vertically from dimmest (top trace) to brightest (*bottom* trace). Each trace was the average of 3–20 sweeps. Light intensities are indicated beside each trace as Log *R**/rod (see "Materials and methods"). **b** The amplitude of each response (total b-wave) was plotted against stimulus intensity (log *R**/rod). *Filled red circles* represent WT response; *filled black triangles* represent knockout mouse response. *Curves* were fitted using the Naka-Rushton function. The light intensities eliciting a half maximum response ($I_{1/2}$) are marked as *K* values on the graph. The intensity response curve has two limbs that represent rod and cone responses, respectively. The two limbs are fitted to *two red curves* by the same function generating 2 distinguishable *k* values, 0.79 for lower limb and 3.34 for upper limb. There is no significant difference between KO *k* values and upper limb *k* values ($P > 0.05$). The strongest stimulus is elicited by a white camera flash, which is calculated as 7.34 log *R**/rod. The *error bars* are equal to the mean ± SEM, $n = 5$

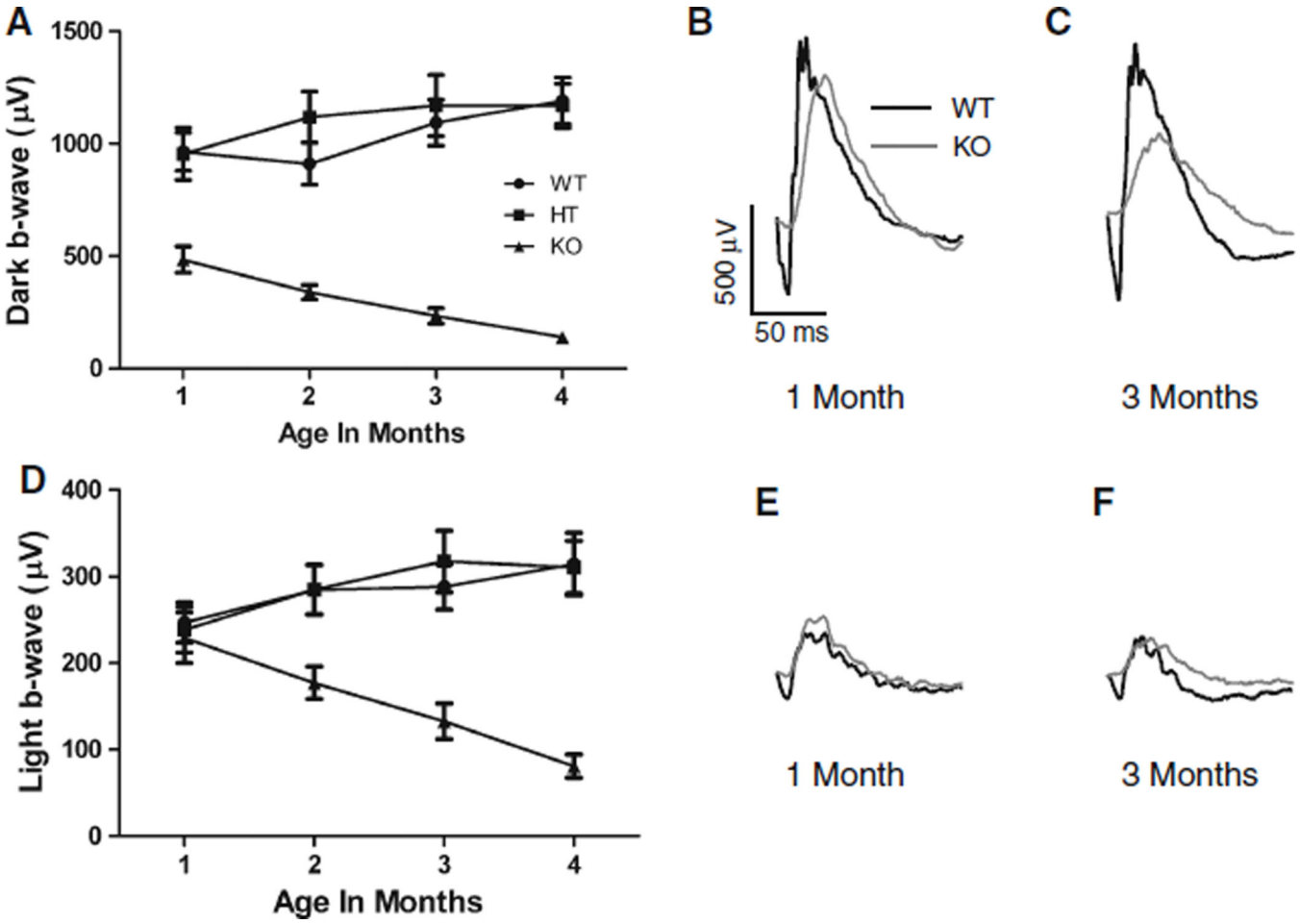

Fig. 4.

Dark- and *light*-adapted b-wave amplitudes plotted as a function of age. **a** Dark-adapted b-wave amplitudes elicited by bright white flashes ($5.63 \times 10^4 R^*$) recorded up to 4 months postnatal in knockout (KO; $n = 11$, *filled triangles*), wild-type (WT; $n = 12$, *filled circles*), and heterozygous (HT; $n = 12$, *filled squares*) mice [*Error bars* = mean ± SEM]. **b, c** Representative *dark*-adapted ERG traces at 1 and 3 months postnatal for WT (*black* trace) and KO (*gray* trace) mice. **d** *Light*-adapted b-wave amplitudes elicited by bright white flashes recorded up to 4 months postnatal. 505-nm background light was set at an intensity necessary to produce 7300 R^*/s per rod. **e, f** Representative *light*-adapted ERG traces at 1 and 3 months postnatal for WT and KO mice

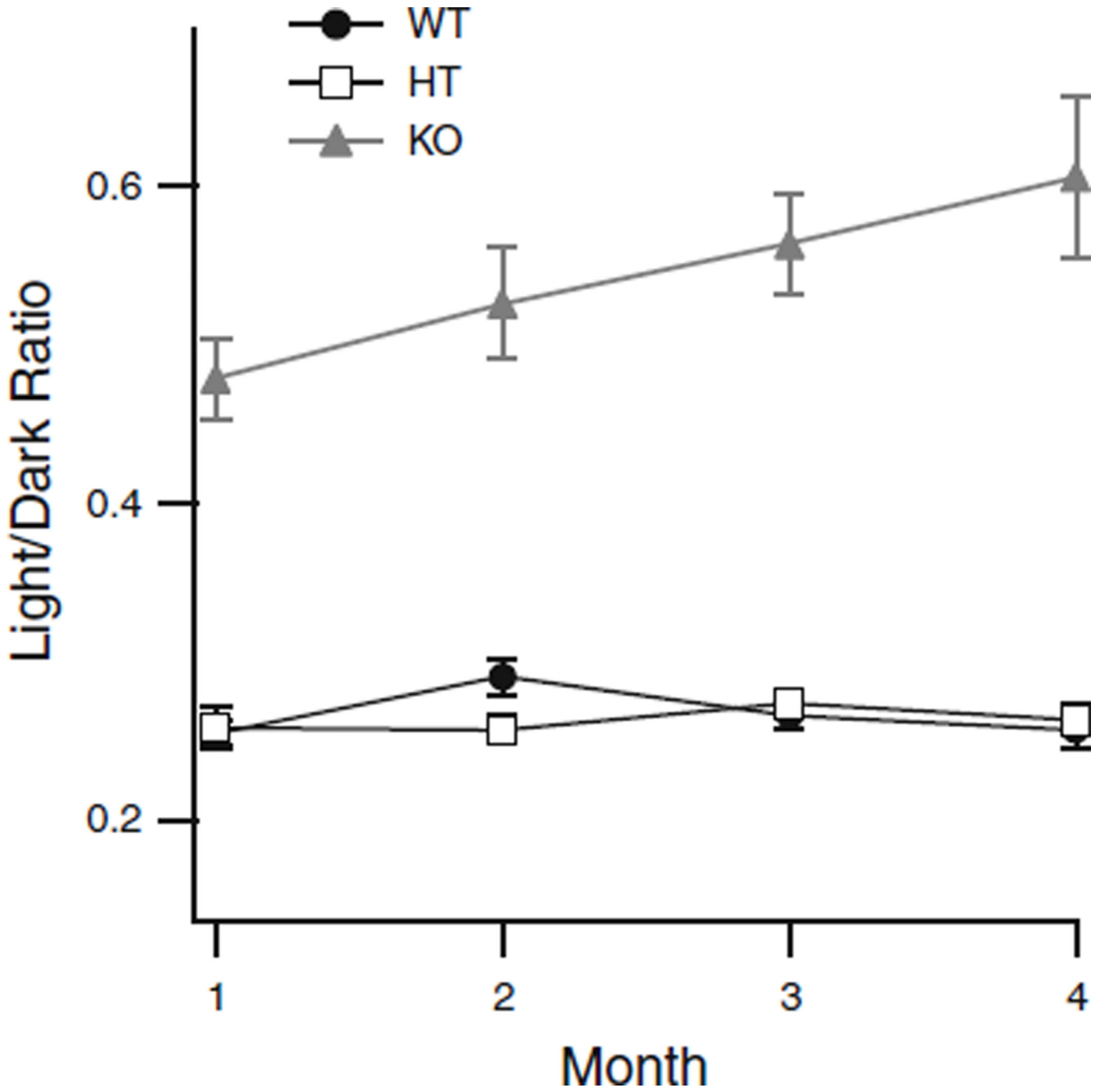

Fig. 5.

Ratio of *light*- to *dark*-adapted b-wave amplitudes plotted as a function of age for: knockout (KO; $n = 11$, *filled gray triangles*), wild-type (WT; $n = 12$, *filled circles*), and heterozygous (HT; $n = 12$, *open squares*) mice (*Error bars* = mean ± SEM, where *bars* are absent error falls within symbol)

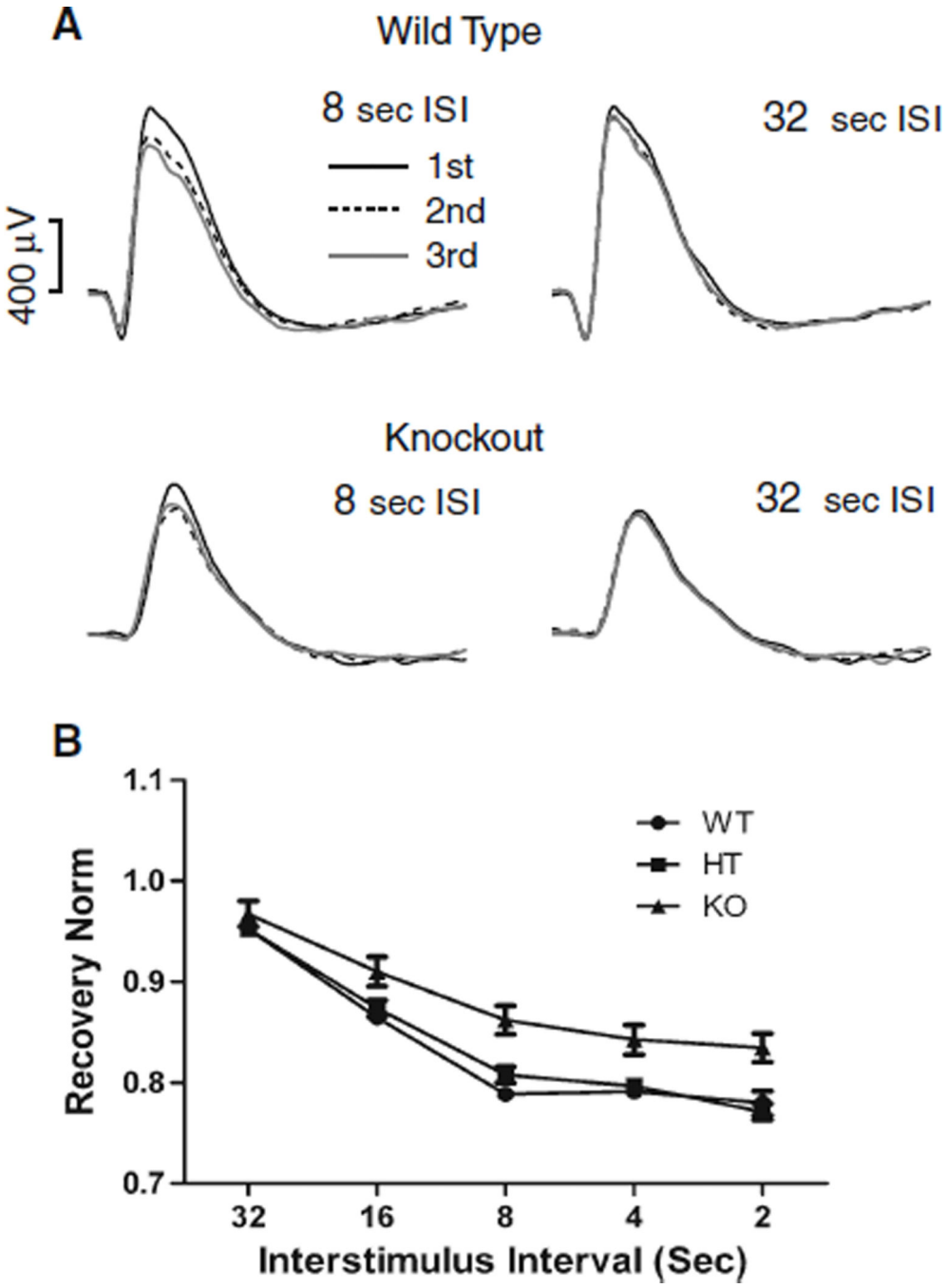

Fig. 6.

PN30 b-wave recovery in WT, HT, and KO mice. Recovery was determined by varying the interstimulus interval (ISI) between trains of three bright 505-nm flashes (1.7×10^4 *R**). The series of interstimulus interval (ISI) values tested were 32, 16, 8, 4, and 2 s. **a** Examples of 8- and 32-s ISI are shown. **b** *Dark*-adapted b-wave recovery values as a function of ISI. Mice were separated into three groups: wild-type (WT, $n = 16$), heterozygote (HT, $n = 17$), and knockout (KO, $n = 15$). These results indicate no significant differences between WT and

HT, and they both are recovering significantly slower than KO mice. *Error bars* = mean ± SEM, where *bars* are absent error falls within symbol

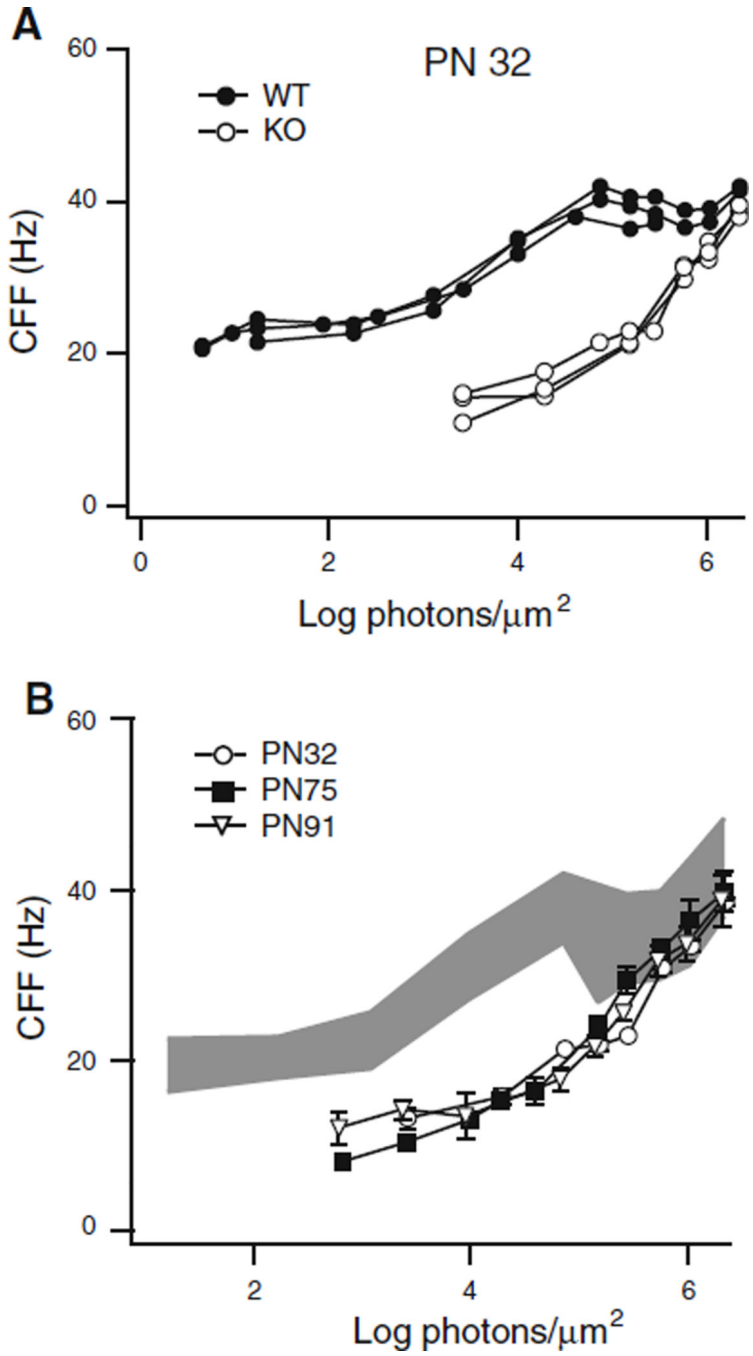

Fig. 7.

Comparison of CFF curves between WT and KO mice. **a** PN32 KO mice (*open circles*) did not respond over the lowest 3 log unit range of stimulus intensities, but at higher intensities compared favorably with the CFF of WT mice (*filled circles*). **b** KO mice CFF curves at three ages: PN32 ($n = 3$, *open circles*), PN75 ($n = 3$, *filled squares*), and PN91 ($n = 3$, *open inverted triangles*). The *gray* region shows the range of WT CFF values (mean ± SD; $n = 9$, 3

animals, each tested 3 times, *Error bars* = mean ± SEM, where *bars* are absent error falls within symbol)

Table 1

Comparison of median photoreceptor counts in 2-month-old mice by location and genotype

2 months old[#]	WT median (IQR)	HT median (IQR)	KO median (IQR)	WT versus HT[*]	WT versus KO[*]
Center	119.0 (109–148)	96.0 (88–119)	106.5 (84–143)	0.23323	0.45231
Inferior nasal	126.5 (112–141)	109.0 (105–116)	138.0 (131–148)	0.21255	0.22720
Inferior temporal	109.5 (96–138)	96.5 (76–104)	130.5 (121–135)	0.046854	0.11015
Superior nasal	146.0 (125–154)	91.0 (74–96)	121 (105–132)	0.058137	0.16696
Superior temporal	123.0 (119–143)	96.0 (77–100)	131.5 (89–139)	0.15653	0.87990

[#] $n = 6$ for all genotypes

IQR interquartile range

[*] *P* value for subunit-specific clustered Wilcoxon rank sum Z statistic, balanced design

Table 2

Comparison of median photoreceptor counts in 4-/6-/7-month-old mice by location and genotype

4/6/7 months old[#]	WT median (IQR)	HT median (IQR)	KO median (IQR)	WT versus HT[*]	WT versus KO[*]
Center	128.0 (115–143.5)	111.5 (96–134)	113.5 (90–128.5)	0.22067	0.32719
Inferior nasal	135.5 (123.5–153)	160.0 (118–176.5)	93.5 (60–132)	0.30818	0.35454
Inferior temporal	141.0 (129.5–154)	135.0 (126.5–142.5)	77.5 (58.5–104.5)	0.73188	0.12134
Superior nasal	115.5 (110–127.5)	129.5 (109–138)	108.5 (91.5–123)	0.60151	0.31731
Superior temporal	130.5 (113.5–138)	108.5 (103.5–127.5)	104.0 (93–108.5)	0.71733	0.27140

[#]HT 4 months old ($n = 4$); WT 7 months old ($n = 4$); KO 6 months old ($n = 2$) + 7 months old ($n = 2$)

IQR interquartile range

[*]*P* value for subunit-specific clustered Wilcoxon rank sum Z statistic, balanced design